Open Peer Review on Qeios

Thermal Remote Sensing: A tool to Determine Temporal Land Surface Temperature in Hawassa City, Ethiopia

Mikias Biazen Molla[1]

1 Hawassa University

Funding: No specific funding was received for this work.

Potential competing interests: No potential competing interests to declare.

Abstract

This investigation was conducted for the estimation of the temporal land surface temperature value using thermal remote sensing of Landsat-8 (OLI) Data in Hawassa City Administration, Ethiopia. Satellite datasets of Landsat-7 (ETM+) on 22nd March 2002 and Landsat-8 (OLI) on 22nd March 2019 were taken for this study. Different algorisms were used to estimate the Normalized Difference Vegetation Index threshold from the Red and Near-Infrared band and the ground earth's surface emissivity esteem is legitimately recovered from the thermal infrared by coordinating with the outcome got from MODIS information. The land use land cover map of the city was prepared with better accuracy using the on-screen classification technique. The spatial distribution of surface temperature of the city ranged from 6.62°C to 22.54°C with a mean of 14.58°C and a standard deviation of 11.25 in the year of March 22nd 2002. The LST result derived from Landsat 8 for March 22nd, 2019, ranges from 11.97°C to 35.5°C with a mean of 23.735 °C and a standard deviation of 16.64. In both years the higher LST values correspond to built-up/settlement and bare/open lands of the city; whereas, lower LST values were observed in vegetation (trees/woodlot, shrubs, and grass forested) areas. Urban expansion (built-up area roads, and other impervious surfaces), decline in vegetation levels due to deforestation, and increasing population density. Increasing evergreen tree and green space coverage, designing and developing city parks, and rehabilitating the existing degraded natural environments are among the recommended strategy to reduce the rate of LST

Mikias Biazen Molla

Department of Geographic Information Sciences, Wondo Genet College of Forestry and Natural Resources, Hawassa University, Hawassa, Ethiopia

Email: mikiasmolla@gmail.com or mikiasb@hu.edu.et

ORCID: https://orcid.org/0000-0002-6694-4579

Keywords: Land SurfaceTemperature, Normalize Difference Vegetation Index, Emissivity, Hawassa, Land use land cover, Urban Heat Island.

1. Introduction

Land surface temperature is the surface temperature of the earth that is directly in contact with the measuring instrument (measured in Kelvin). As defined by Anandababu et al. (2008) land surface temperature is the surface temperature of the earth's crust where the heat and radiation from the sun are absorbed, reflected, and refracted. Land surface temperature varies with a transition in the environment and other human behaviors, so forecasting precisely is difficult. Earth's surface energy balance, and thermal properties of the surface and atmospheric conditions affect the land surface temperature dramatically (Guo et al. 2012; Orhan et al. 2014). Urbanization is one of the most important factors for the socio-economic development of the city (Dociu and Dunarintu, 2012; Nimish et al. 2018).

Currently, urbanization has dramatically increased greenhouse gasses and reshaped the environment, and has major climatic effects at all scales owing to the gradual transition of natural land use into an urban region (Yan et al. 2002; Yıldırım et al. 2011; Orhan et al. 2014). Unplanned urbanization is the product of rapid growth in size and speed, resulting in decentralized and scattered construction (urban expansion) (Bharath et al. 2014) and various environmental effects (Mohan et al. 2011). Land surface temperature plays an important role in research on the effects of urban heat islands, and environmental monitoring (Lu and Weng 2006; Muhammad et al. 2018). Land surface temperature is the main factor in the measurement of a given location's maximum and lowest temperature.

Urban Heat Island (UHI) definition and classification are usually based on spatially varying land surface temperature, due to non-homogeneity of the surface cover and other atmospheric factors (Jeevalakshmi et al. 2017). Remote sensing is useful for understanding spatio-temporal land cover changes in terms of surface radiance and emissivity data in relation to the basic physical properties (Tran et al. 2006; Orhan and Yaka 2016). Land surface temperature, calculated from remote sensing data, is used in many areas of science; such as; hydrology, agriculture, climate change, urban planning, etc. To evaluate the environmental problem, it is important to obtain surface temperatures and use them in various experiments (Orhan et al. 2014).

Many researchers showed that Landsat having a medium-resolution satellite is the only source of earth surface temperature worldwide since 1972 (Amiri 2009; Guo et al. 2012; Orhan and Yaka 2016; Avdan and Jovanovska 2016). For the Land Surface Temperature study, Landsat 8 is the most important source of data (Muhammad et al., 2018). It was launched on the 11th of February 2013 into space with two instruments on board, the Operational Land Imager (OLI) and the Thermal Infrared Sensor (TIRS) (Anandabablunu et al. 2008; Muhammad et al. 2018).

According to Jeevalakshmi et al. (2017), OLI gathers data at a spatial range of 30 m, with eight bands distributed in the electromagnetic spectrum's visible and near-infrared and short-wave infrared regions, and an additional panchromatic band of 15m spatial resolution. TIRS senses the TIR radiance at a spatial resolution of 100m using two bands located in the atmospheric window between 10 and 12 µm (Muhammad et al. 2018; Anandababu et al. 2008).

This study was conducted in Hawassa City Administration, Ethiopia, which is the central city of the Southern region. Multi-temporal thermal image series acquired by Landsat -5 TM/8-OLI were used. The main objective of this study was to estimate the temporal land surface temperature using thermal remote sensing.

2. Material and Methods

2.1. Description of Study Area

This study area was carried out in Hawassa town and the surrounding area. It is located in the southern Nations, Nationalities, and Peoples (SNNP) regional state. It is a city in Ethiopia, on the shores of Lake Hawassa in the Great Rift Valley. It is found at a distance of 273 km south of Addis Ababa, the city that is the most rapidly expanding city in the country. Geographically, it is located on latitude and longitude of $6^0$55'N $38^0$25'E and $7^0$5'N $38^0$33'E in geographical coordinate Systems respectively. The city is one of the industrial cities of the country and has become the most beautiful city, tourist attractive city in the country. The city administration has an area of 157.2 Square km, but the overall study area has an area of 560 square Km. The mean annual rainfall was estimated to be 973mm. The mean annual temperature area was estimated to be 27.45^0C at maximum temperature, 13.04^0C at minimum temperature, and 20.25^0C at the mean temperature. The monthly average maximum temperature of the area varies from 24.57^0C to 29.99^0C, the monthly average minimum temperature of the area varies from 10.36^0C to 14.58^0C, and the monthly average mean temperature of the area varies from 19.32^0C to 21.57^0C.

Based on the 2007 census conducted by the Central Statistical Agency of Ethiopia this town has a total population of 157,139 out of this 81,020 are men and 76,119 women are living in the city (CSA 2007). Based on the result of the housing and population census from May 2007 to 2016 the projected population of Hawassa city administration is 371,826 people out of this 191,352 was male and 180,474 are females. On the basis of the CSA report, the total population of the city administration is 242,489 people living in urban areas while the reaming 129,337 people live in rural areas of the administration (Socio-Economic Profile of the City Administration 2016).

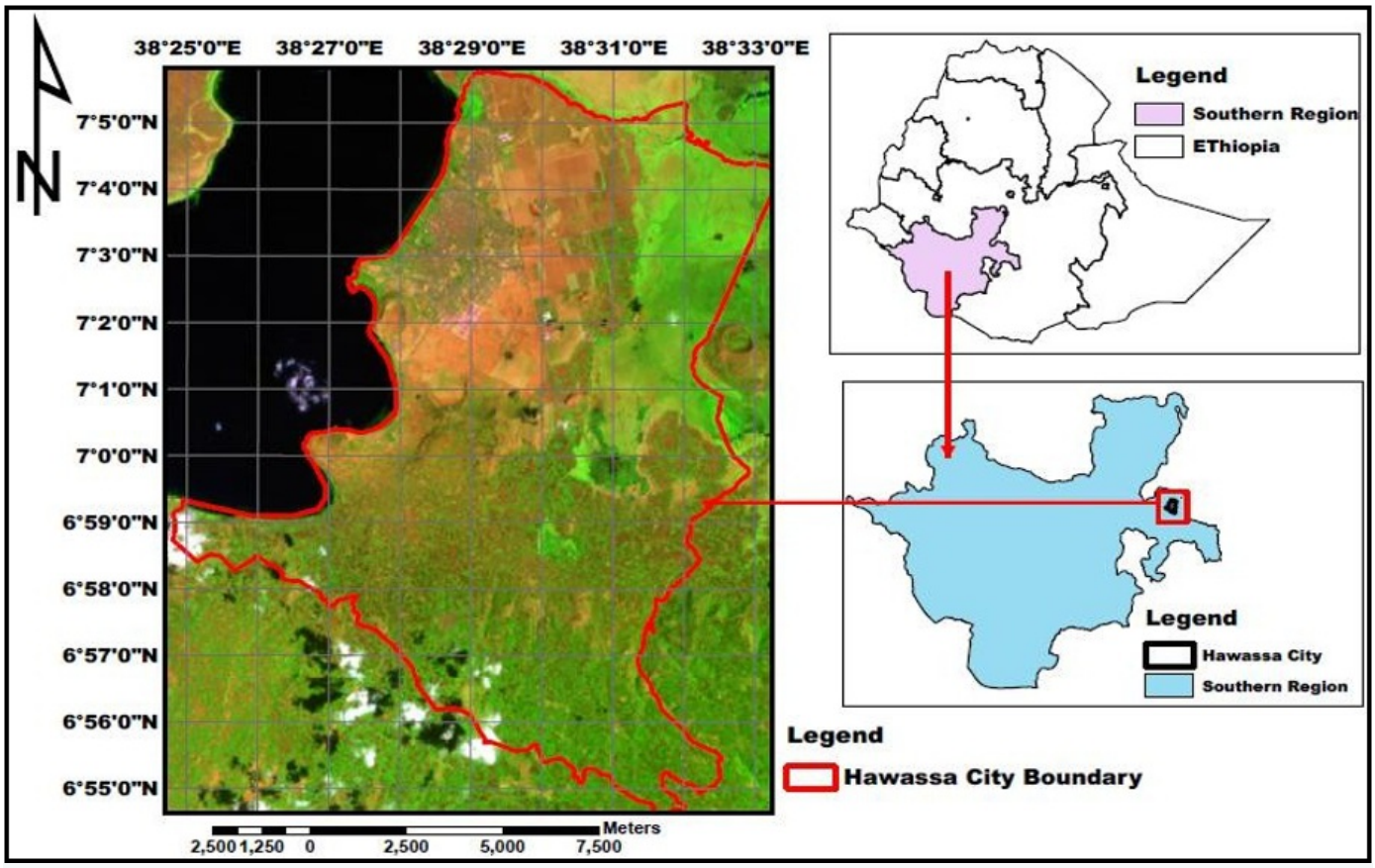

Figure 1. *Map of the study area*

2.2. Data Used

A Landsat 8 OLI image is one of the Landsat series of NASA. For this study January, February, and March 2019 (Path/Row-168/55) pertaining to the study area were used to estimate the temporal land surface temperatures. In the present study, bands **10** were used to estimate brightness temperature, and bands 4 and 5 were also used to generate normalized difference vegetation index of the study area. Landsat 8 provides metadata of the bands such as thermal constant, rescaling factor value, etc., which can also help to calculate land surface temperature. Landsat 8 Bands, Wavelength, and Resolution are shown in Table 1.

Table 1. Characteristics of Landsat 8 OLI and TIRS

Band Designations	Wavelength (μm)	Resolutions (m)
Band 1 (Coastal Aerosol)	**0.43-0.45**	**30**
Band 2 (Blue)	**0.45-0.51**	**30**
Band 3 (Green)	**0.53-0.59**	**30**
Band 4 (Red)	**0.64-0.67**	**30**
Band 5 (Infrared)	**0.85-0.88**	**30**
Band 6 (Short wave Infrared)	**1.57-1.65**	**30**
Band 7 (Short wave Infrared)	**2.11-2.29**	**30**
Band 8 (Panchromatic)	**0.50-0.68**	**15**
Band 9 (Cirrus)	**1.36-1.39**	**30**
Band 10 (Thermal Infrared)	**10.6-11.19**	**100**
Band 11 (Thermal Infrared)	**11.50-12.51**	**100**

Source: compiled by Author

Hand-held GPS (Global Positioning System) was used to collect necessary ground truth data and the classified outputs were validated using Google Earth. All activities have been conducted in the Free and Open Source (FOSS) Quantum GIS framework using Semi-Automatic Classification Extension 4.3.3 for the classification and calculation of land surface temperatures.

2.3. Methodology

Techniques of Thermal Infrared (TIR) remote sensing have been used to study urban climate and environment and especially for assessing and estimating land surface temperature patterns and their relationship with surface characteristics (Weng et al. 2004; Jeevalakshmi et al. 2017). The study utilized the potentials of a Semi-Automatic Classification plugin integrated with Open Source GIS package Quantum GIS for image acquisition, pre-processing, image classification, and derivation of land surface temperature from land surface emissivity values. A detailed description of the methodology is outlined here (Figure 1). Image acquisition and Pre-processing of cloud-free Landsat a scene (Path/Row-168/55) was downloaded. The whole approach used for the proposed work is shown in **Figure 2**. This technique can only be used to process LANDSAT 8 data. In this research, Band 10 is used in this study to calculate surface temperature, and it is calculated using bands 4 and 5 to normalize the discrepancy vegetation index.

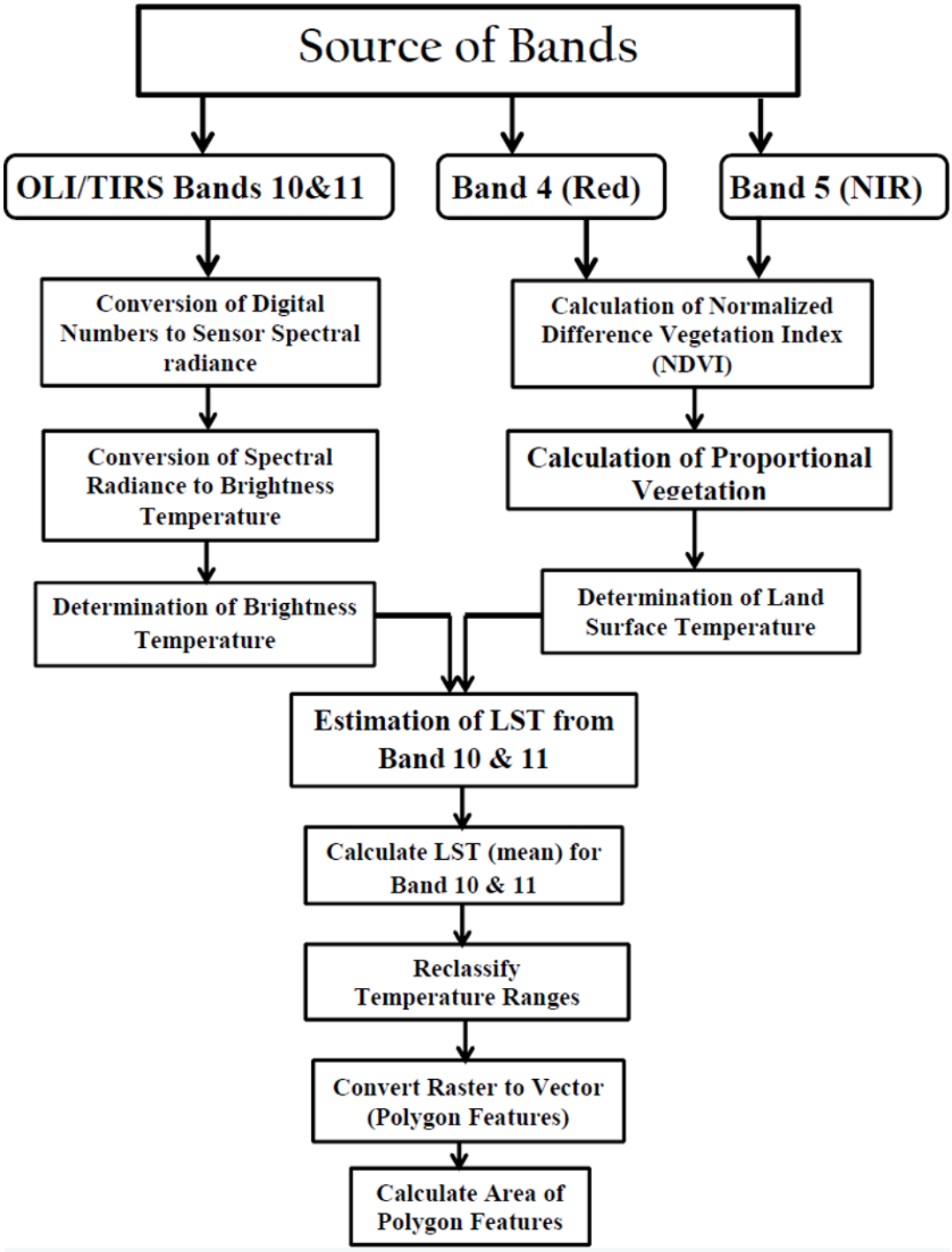

Figure 2. ***Analytical flow*** *diagram of Land SurfaceTemperature retrieval*

2.4. Method of Data analysis

There are several steps or analytical procedures to be followed in order to conduct LST estimation and analysis. Conversion of DN values into Top of Atmosphere (TOA) Radiance is the first step in land surface temperature estimation. In this algorithm, the satellite data were geometrically corrected, and band ten was used as input data. In this activity radiance, the rescaling factor is very important to retrieve the top of atmospheric (TOA) spectral radiance from Thermal Infra-Red Digital Numbers. In order to estimate the land surface temperature from the Landsat-8 thermal infrared band

data, DN of sensors are converted to spectral radiance using the following equation (Barsi et al. 2014; USGS 2013; Jeevalakshmi et al. 2016; Ren et al. 2015; Julia 2014; Wang et al. 2015).

$$= * + - \quad (1)$$

Where:

- ML represents the band-specific multiplicative recalling factor
- Qcal is the Band 10 image
- AL is the band-specific additive rescaling factor
- O*i* is the correction value for band 10 (Barsi *et al.* 2014)

After converting DN values to at-sensor spectral radiance, the TIRS band data should be converted to Top of atmosphere brightness temperature (BT) using the thermal constants given in the metadata file. The following equation is used as a tool in this algorism to convert reflectance to brightness temperature (USGS 2013).

$$TB = \frac{}{(+)} \quad (2) \text{ in Kelvin (K)}$$

For obtaining the results in Celsius, the brightness temperature is revised by adding the absolute zero (–273.15∘C) (Juan-Carlos et al. 2008; Orhan et al. 2014; Avdan and Jovanovska 2016). That means when the spectral radiance was converted to brightness temperature by assuming the earth's surface is a black body (Eq. 3) (Orhan et al. 2014; Chander et al 2009; Coll et al 2010).

$$TB = \frac{}{(+)} - 273.15 \quad (3) \text{ degree Celsius}$$

Where:

- BT = Top of atmosphere brightness temperature (K/°C)
- Lλ = TOA spectral radiance (Watts/(m2 * sr * μm))
- K1= Band specific thermal conversion constant from the metadata (K1_constant_Band_x, where x is the thermal band number)
- K2= Band specific thermal conversion constant from the metadata (K2_constant_Band_x, where x is the thermal band number)

On the other hand, Normalized Difference Vegetation Index is very essential to identify different land cover types of the study area. Normalize Difference Vegetation Index ranges from -1.0 to +1.0. Normalize Difference Vegetation Index is calculated on a per-pixel basis as the normalized difference between the red band (0.64 - 0.67 μm) and near-infrared

band (0.85-0.88 μm) of the images using the following equation (Muhammad et al 2018).

$$= \frac{- \quad -}{- \quad +} \quad or = \frac{-}{+} \qquad (4)$$

Where:

- RED= DN values from the Red band (Band 4)
- NIR= DN values from the Near-Infrared band (Band 5)

The next step is calculating proportional vegetation (Pv), this was done using the normalized difference vegetation index values or results obtained in the above step. This proportional vegetation helps to estimate the area under each land cover type in the study area (Jeevalakshmi et al 2017; Muhammad et al 2018). Thus, proportional vegetation (Pv) can be calculated using the following equation (5).

$$= \left(\frac{\text{Normalize Difference Vegetation Index} - \text{Normalize Difference Vegetation Index}}{\text{Normalize Difference Vegetation Index} \quad - \text{Normalize Difference Vegetation Index}}\right) \qquad (5)$$

Where:

- PV = Proportion of Vegetation
- Normalize Difference Vegetation Index = DN values from NormalizeDifference Vegetation Index Image
- Normalize Difference Vegetation Index min = Minimum DN values From Normalize Difference Vegetation Index Image
- Normalize Difference Vegetation Index max = Maximum DN values from Normalize Difference Vegetation Index Image

The computation of land surface emissivity (LSE) is very critical to estimate the land surface temperature of the study area. LSE is describe the radiative absorption ability of a surface in a long wave radiation spectrum (Jose et al. 2008) and transmissions of thermal energy across the surface into the atmosphere (Ugur and Gordana, 2016). In addition, LSE is largely dependent on the target surface top layer such as the type of soil, surface roughness, and nature of vegetation cover (Stathopoulou and Cartalis 2007; Ren et al 2015). Land surface emissivity is the Earth's average surface factor emissivity determined from the standardization of vegetation index values for variations. Corrections for emissivity (e) have been applied to the radiant temperatures according to the nature of land cover (Jeevalakshmi et al 2017). In general, vegetated areas have given a value of 0.95 and non-vegetated areas 0.92 (Weng and Lu 2008). The determination of the ground emissivity is calculated conditionally as suggested by Julia et al. 2014; Sobrino et al. (2004), and Stathopoulou and Cartalis (2007):

$$= \quad + \quad (\quad - \quad) + \qquad (6)$$

Where:

- ε = Land Surface Emissivity
- εvλ = emissivity of vegetation
- εsλ= emissivity of soil
- PV = proportion of vegetation
- Cλ = surface roughness taken as a constant value of 0.005

Where εv and εs are the vegetation and soil emissivity respectively, C is the surface roughness taken as a constant value of 0.005 [16]. Studies conducted by Jose et al. (2008) show that the emissivity of water bodies is of utmost stability in comparison with land surfaces. Since the emissivity depends on the wavelength, the Normalize Difference Vegetation Index can be used to estimate the emissivity of different land surfaces in the 10-12 μm range (Jeevalakshmi et al 2017; Muhammad et al., 2018). According to Rajeshwari and Mani, (2014) report the average emissivity of four major land cover types can be considered in Band 10 as, when the Normalize Vegetation Difference Index is less than 0, it is marked as water and the emissivity value of 0.991 is given for Normalizing Vegetation Difference Index values from 0 to 0.2.
This is considered that the land cover type is soil, and the emissivity value of 0.966 is assigned. While, values between 0.2 and 0.5 are considered as mixture of soil and vegetation cover and the above equation (Mallick et al 2012; Rajeshwari and Mani 2014) is applied to calculate the emissivity. In the last case, when the Normalize Difference Vegetation Index value is greater than 0.5, it is considered vegetation cover, and the value of 0.973 is assigned (Rajeshwari and Mani 2014; Jeevalakshmi et al., 2017).
Calculating Land Surface Temperature is the final step in this algorism. The surface temperature value of the study area can be calculated as the following equation (7)

$$LST = \left(\frac{BT}{1 + W} * \frac{BT}{p} * ln(e)\right) \qquad (7)$$

Where: BT = Top brightness value of atmospheric temperature (°C), W = Wavelength of emitted radiance in meters (for which the peak response and the average of the limiting wavelengths (λ = 11.5lm). Jeevalakshmi et al (2017) and Orhan and Yaka (2016) are used, p = h * c/r (1.4388 * 10^{-2}m K), r = Boltzmann constant (1.38 * 10^{-23} J/K), h = Planck's constant (6.626 * 10^{-34} J s), and c = velocity of light (2.998^{-108} m/s) and e = emissivity (ranges between 0.97 and 0.99) (Eq. 6). For ease of comprehension, the above-derived land surface temperature s' unit was converted to degree Celsius using the relation of 0 _C equals 273.15 K.

2.5. Validation of retrieved Land Surface Temperature

Validation is required for independent assessment of the accuracy and uncertainty of the derived output (Nikam et al.

2016). As the Earth's surface temperature is determined from thermal remote sensing datasets utilizing dynamic methods and underlying hypotheses regarding atmospheric parameters, it is also important to determine its precision, which is beneficial for both consumers and engineers. (Li et coll., 2013). Normal land surface temperature products of the same region and same time span can be used to confirm the obtained surface temperature values. Yet due to the complex existence of land surface temperature, both spatially and temporarily, ground-based values cannot be obtained to cross-validate the temperature of the collected surface. Furthermore, owing to the non-availability of observed surface temperature details, the cross-validation technique was used to confirm the recovered surface temperature of the earth; thus, we used regular data sets of Landsat 8- OLI earth surface temperature products with precision within 1oK range (Weng et al. 2004) to confirm the earth surface temperature of Landsat 8 satellite image.

3. Results and Discussion

The present study has been conducted to analyze the effectiveness of multispectral satellite data to retrieve land surface temperature using spectral classification techniques. Landsat-7 from 22nd March 2002 and Landsat-8 of 22nd March 2019 were taken as sources of data for this study. The investigation registered land use/land front of the investigation territory for two periods: 2002 and 2019 relating to land surface temperature item datasets to analyze the adjustment in land surface temperature over the investigation region. Four classes of land cover are identified in the study areas, which are built-up includes, agriculture, vegetation, and open land (land other than farm or agricultural land which was left open) (Table 2).

It has been seen that there is an increment in the built-up area from 2002 to 2019 and the physical expansion of the area has expanded from 1216.75 ha to about 7.61% of the total area in 2002 to 3620.18ha (22.64%) in 2019. Thus, a net expansion of 2403.43ha (15.03%) is noticed over the time period of 17 years (Table 2). This change in the built-up area is attributed to human settlement, government institutions (educational and health institutions, and other sectoral offices), and different industries such as textile, leaser, food processing factories, horticulture, industry park, etc. Further, there is a decrease in agricultural land, forested area, and an increase in vegetation and barren land. This may be attributed to changes in land use for encroachment in the forested area, cash crop development in the periphery of the city, and expansion of developmental projects in the agricultural land in the study area. The consolidated status of land use/land cover for the years 2002 and 2019 is given in **Table 2** and the same has been shown in**Figure 4**.

Table 2. Status of Land use-LandCover Classes. Source: Authors, 2019.

Land cover class	March 2002		March 2019	
	Area in ha	Percentage (%)	Area in ha	Percentage (%)
Built-up/settlement	1216.75	7.61	3620.18	22.64
Agricultural Land	2239.50	14.01	4026.90	25.19
Vegetation	10138.53	63.42	8054.42	50.38
Barren/open land	2392.72	14.97	286.00	1.79
Total	**15987.50**	**100.00**	**15987.50**	**100.00**

As stated above the land use-land cover classes are categorized into four classes. These include built up includes (urban area, roads, and small villages/settlements); agriculture (cultivated land and Industrial farms); Vegetation (trees/woodlot, shrubs, and grass); and open land (land other than farm or agricultural land which was left open).

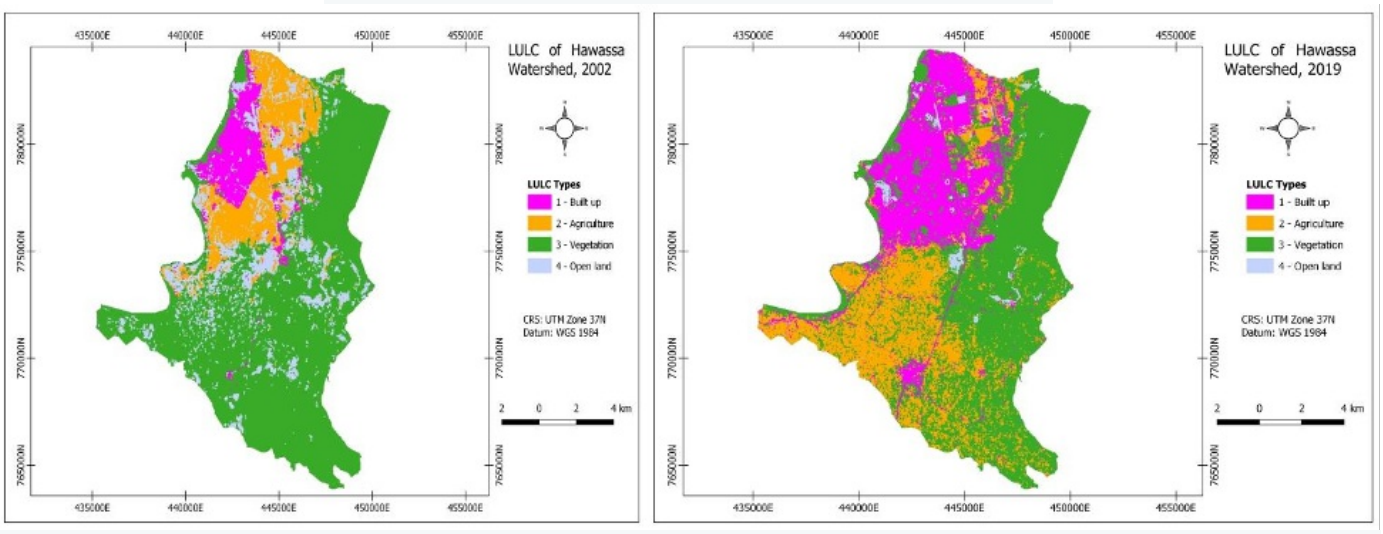

Figure 3. *Land use-landcover of the study area (Year 2002 (A) and 2019 (B)).* Sources: computed by Authors.

In this research Normalize DifferenceVegetation Index values were determined for the years 2002 and 2019 using satellite images respectively. The value for Normalize Difference Vegetation Index for the year 2002 ranges from **-**0.534 (low) to 0.566(high); the forested area has high values of Normalize Difference Vegetation Index followed by agricultural land in both 2002 and 2019 (**Figures 3 and 4**). For the year 2019, Normalize Difference Vegetation Index value ranges fro m **-**0.121 (low) to 0.543 (high). This clearly shows the healthy vegetative condition in the year 2002 as compared to 2019 (**Figures 3 and 4**).

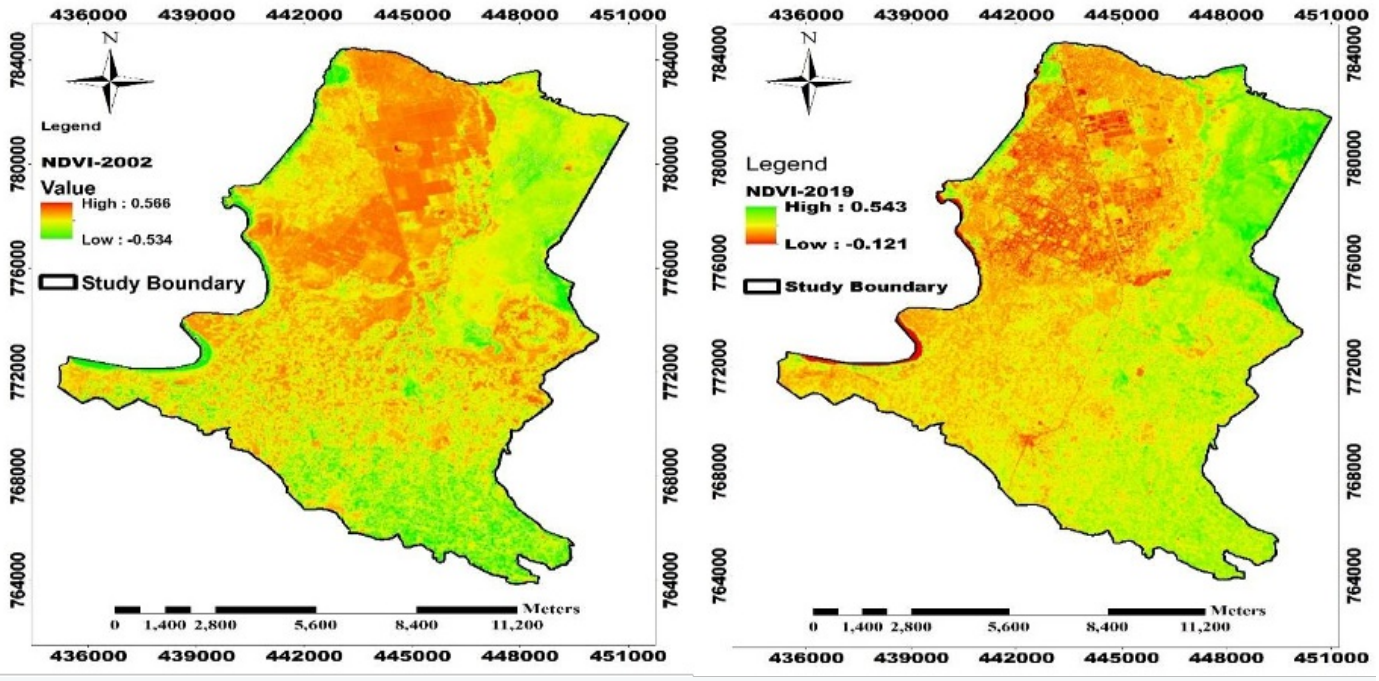

Figure 4. *Normalize Difference Vegetation Index derived from Landsat -7 (A) and Landsat- 8 (B) of March 22 nd, 2002 and 2019 respectively.*

Sources: Computed by Author.

Land Surface Temperature Analysis

In this study, Landsat 7 (ETM+) and Landsat 8 TIRS data have been utilized for estimating the land surface temperature of the study area. A Single channel (SC) equation-based method was used to estimate land surface temperature. Land surface temperature estimation is shown in Figure 5 respectively. The land use/land spread map (Figure 3) was created for the years 2002 and 2019 and has been utilized in the current investigation to look at the land surface temperature for particular years. The spatial distribution of LST of Landsat 7, dated 22nd March 2002 shows that the LST ranges from a minimum of 6.62°C to a maximum of 22.54°C with a mean value of 14.58°C and a standard deviation value of 11.25. The higher LST relate to developed/settlement and exposed/open place that is known for the study area; though, lower LST esteems were seen in forested and agricultural place where there is the investigation territory (Figure 3 and 5). Such land surface temperature figures are often accompanied by the values of the Normalize Vegetation Differential Index (Figure 4 above).

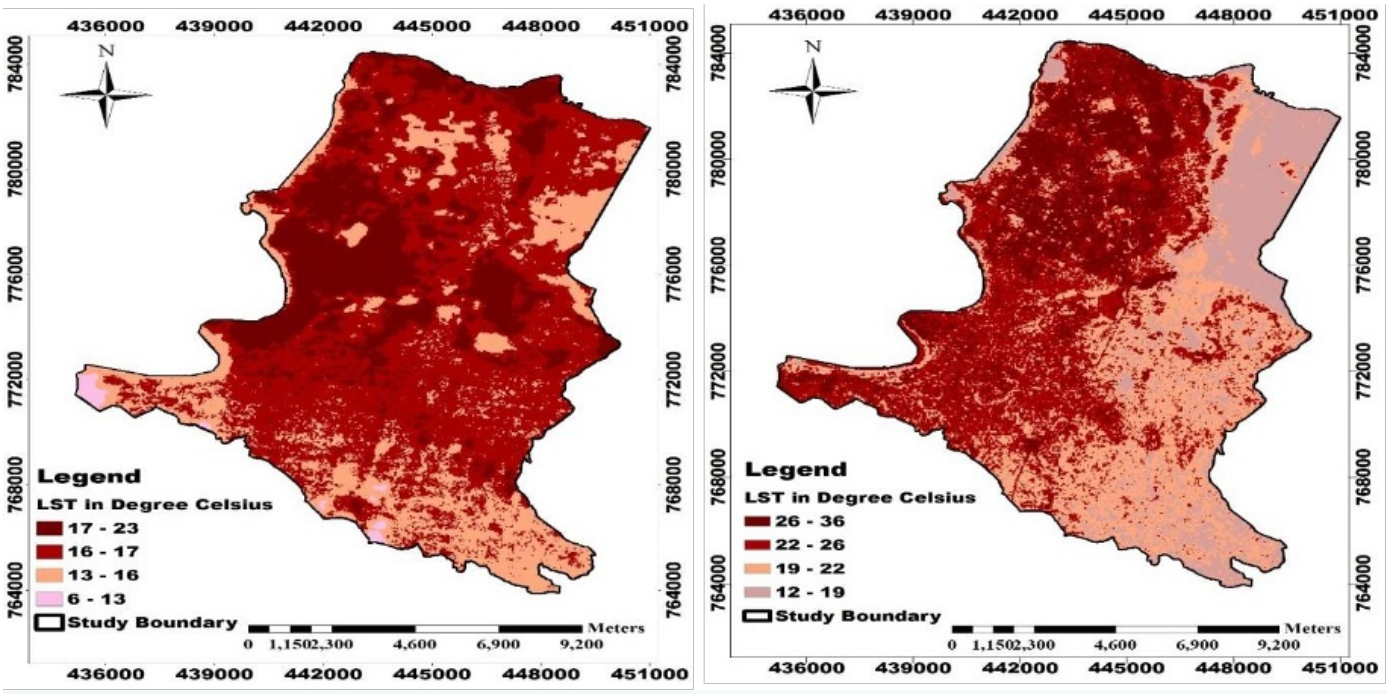

Figure 5. *Spatial Distribution of land surface temperature of Landsat -7 data of 22nd March 2002 and Landsat -8 data of 22nd March 2019.* Sources: Computed by Authors.

The land surface temperature results obtained from Landsat-8 for March 22nd, 2019 show the highest value (35.5°C), which is observed in the center of the city, and besides, barren land and villages and the areas where construction is taking place. Whereas, the lower land surface temperature value was observed at about 11.97°C in the forested area of the study area, while the built-up areas were increased to 35.5°C (Figures 3 and 5). The mean land surface temperature was observed to be 23.735°C and a standard deviation of 16.64 for March 22nd, 2019 land surface temperature estimates. The hot and cold spot areas in the study region represent the highest and lowest land surface temperature values. It is observed that the surface area under the higher land surface temperature values increased from 2002 to 2019.

It is remarkable that the minimum and maximum temperature values of the year 2019 are very much higher than that observed on March 22nd, 2002. That means the range of lowest temperature increased to 11.97°C in 2019 from 5.62°C in 2002, similarly, the range of maximum temperature also increased to 35.5°C in 2019 from 20.21°C in 2002. These could be attributed to the change in the urban environment from natural to artificial or manmade surface/environment over the last 17 years.

Figure 6 simply illustrated the trends of minimum and maximum temperature in the study area (from 2012-2107). As observed from the figure, the values of both the minimum and maximum temperatures show an increasing trend over time due to the expansion of the city and the reduction of forests, vegetation, and other natural environments. Starting from October to April the temperature has shown a higher value than the rest months. On the other hand, from May to September the maximum temperature becomes lower than others, particularly, in June, July, and August, the maximum temperature has a lower value, because these seasons mainly know as a rainy season in the country as well as the study area.

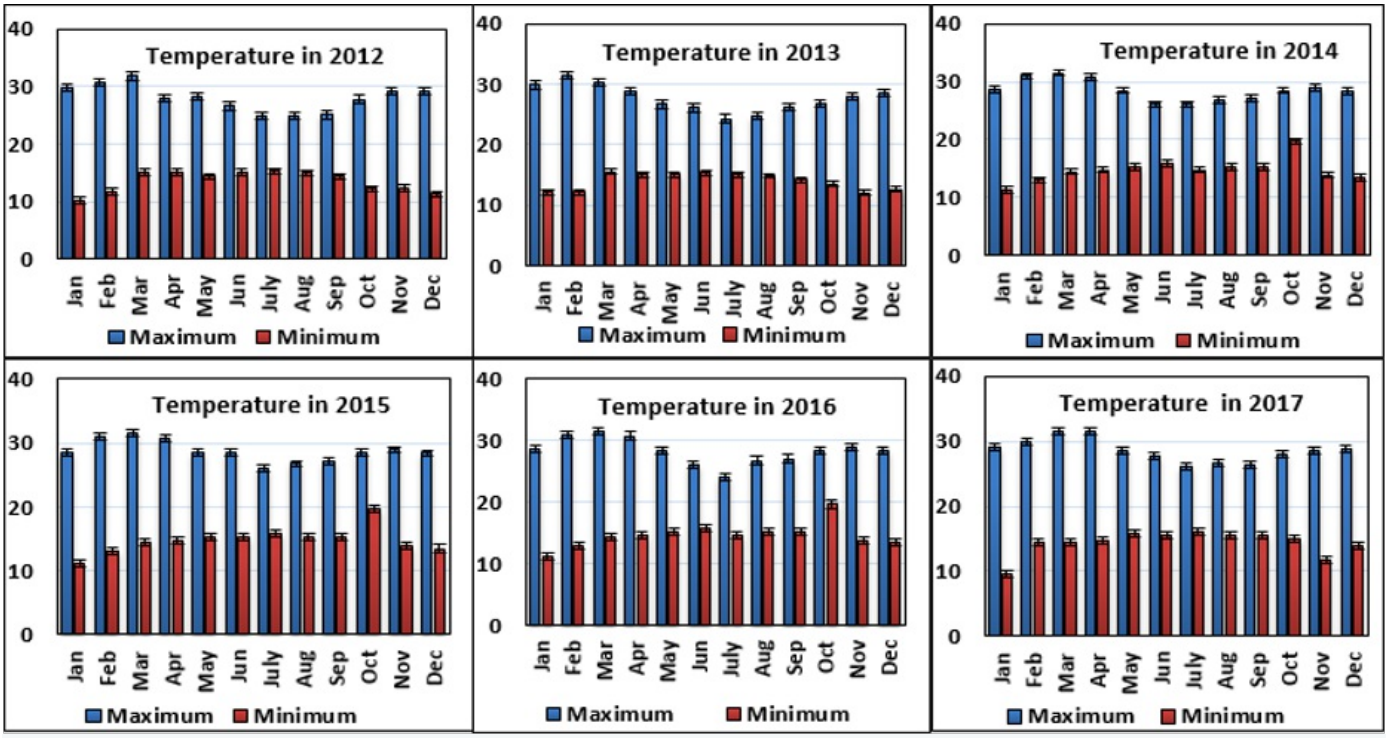

Figure 6. *Minimum and Maximum Temperature Trends from 2012-217*

Sources: Southern Nation Nationalities Peoples Region Time Series Statistical Abstract, 2018

However, in most cases of the selected years (**Figure 6**) the minimum temperature shows a lower value in November, December, January, and February, the rest months show a constant value trend. This implies that the value average temperature increased over time due to the expansion of impervious surfaces in the expense forest, vegetation, agriculture, and other natural environments. On the other hand, the conservation of the natural environment (urban forests, green space, green belts, e.t.c) has become deceased. However, detailed climate change studies will be required to arrive at conclusion in relation to increasing and decreasing existing temperatures.

The estimated land surface temperature from Landsat products using a single channel was validated using MODIS land surface temperature products of the same date and area. Additionally, the associated land use / land cover transition was also examined to understand the effect of land use changes on land surface temperature behavior. The land surface temperature derived from MODIS data products ranges from a minimum of 8.75°C to a maximum of 16.55°C for March 22nd, 2002 with a mean of 24.76°C and a standard deviation of 11.03; and a minimum of 13.11°C to a maximum 36.43°C for March 22nd, 2019 with mean of 24.77°C and standard deviation 16.45. This estimate was not found close to the land surface temperature estimate derived from Landsat 7 and 8. The MODIS land surface temperature image has a larger spatial resolution of 1 km compared to the land surface temperature recovered using Landsat 7 (ETM+) and Landsat 8(OLI) TIRS with a resolution of 30m. However, the high-temperature zone was found to be the same, i.e. built-up area (urban area, roads, and small villages/settlements) with developmental activity and open land (land other than farm or agricultural land which was left open, indicates reasonable reliability of the retrieved land surface temperature. Overall, the hot and cold areas identified in MODIS image products fit the Landsat land surface temperature products reasonably well. These findings can be reinforced by correlation and sensitivity analyses for validation purposes and MODIS data re-

sampling methodology to avoid the issue of coarser resolution on land surface temperature estimates.

Conclusion

This study investigated the spatial variability of land surface temperature over Hawassa city Administration located in the southern part of Ethiopia. This study examines the change in land surface temperature over different land use/land cover of the area over the period of time (17 years) where developmental activities alter the natural ecosystem. The land surface temperature was derived using Landsat-7 Enhanced Thematic Mapper Plus for March 2002 and Landsat-8 for March 2019. Normalize Difference Vegetation Index threshold was used to measure the emissivity of land surfaces. The spatial distribution of land surface temperature of Landsat 7 of 22nd March 2002 was observed in the rages of a minimum of 6.62°C to a maximum of 22.54°C with a mean of 14.58°C and standard deviation of 11.25; whereas, for Landsat 8 (OLI), of 22nd March 2019 the land surface temperature estimates range from minimum range from 11.97°C to maximum 35.5°C with the mean of 23.735°C and standard deviation of 16.64. The land surface temperature values derived from the analysis depend on the distribution of the land cover and are negatively correlated with the abundance of vegetation. The result reveals that the higher vegetative cover such as forested areas, dense and sparse vegetation, trees/woodlot, shrubs, and grassland, agricultural croplands bring down the surface temperature. Whereas, areas covered by built-up area and land developmental activities (urban area, roads, and small villages/settlements) bare land or open space increases the surface temperature of the city. The rapidly growing urban agglomeration and degradation of the natural environment (green space) are the main causes of the increment of land surface temperature in the city. The outcome of this research is to demonstrate the role of geospatial technologies in land surface temperature estimation and this would help to assist studies on the urban environment and effective urban land use planning.

Competing interests

The author declares that they have no competing interests.

Author contributions

Mikias Biazen Molla developed the overall methodology section, the main analysis framework, collecting primary and secondary data, and carried out the multi-criteria analysis. Finally, the author read and approved the final manuscript.

Ethical approval

This article does not contain any studies with human participants or animals performed by any of the authors.

Informed consent

None

Acknowledgment

The author would like to thank Mr. Tekelu B and Mr. Gezahegn G for their help in various ways.

References

- Amiri, R., Weng, Q., Alimohammadi, A., & Alavipanah, S. K. (2009). Spatial–temporal dynamics of land surface temperature in relation to fractional vegetation cover and land use/cover in the Tabriz urban area, Iran. Remote sensing of environment, 113(12), 2606-2617.
- Anandababu, D., Purushothaman, B. M., & Suresh, B. S. (2018). Estimation of land surface temperature using Landsat 8 data. International Journal of Advance Research, Ideas and Innovations in Technology, 4(2), 177-186.
- Avdan, U., & Jovanovska, G. (2016). Algorithm for automated mapping of land surface temperature using LANDSAT 8 satellite data. Journal of Sensors, 2016.
- Aithal, B. H., Vinay, S., & Ramachandra, T. V. (2014, December). Prediction of spatial patterns of urban dynamics in Pune, India. In 2014 Annual IEEE India Conference (INDICON) (pp. 1-6). IEEE.
- Burgan, R. E. (1993). Monitoring vegetation greenness with satellite data (Vol. 297). US Department of Agriculture, Forest Service, Intermountain Research Station.
- Chander, G., Markham, B. L., & Helder, D. L. (2009). Summary of current radiometric calibration coefficients for Landsat MSS, TM, ETM+, and EO-1 ALI sensors. Remote sensing of environment, 113(5), 893-903.
- Coll, C., Galve, J. M., Sanchez, J. M., & Caselles, V. (2009). Validation of Landsat-7/ETM+ thermal-band calibration and atmospheric correction with ground-based measurements. IEEE Transactions on Geoscience and Remote Sensing, 48(1), 547-555.
- Jeevalakshmi, D., Reddy, S. N., & Manikiam, B. (2016, April). Land cover classification based on NORMALIZE DIFFERENCE VEGETATION INDEX using LANDSAT8 time series: a case study Tirupati region. In 2016 International Conference on Communication and Signal Processing (ICCSP) (pp. 1332-1335). IEEE.
- Dociu, M., & Dunarintu, A. (2012). The socio-economic impact of urbanization. International Journal of Academic Research in Accounting, Finance and Management Sciences, 2(1), 47-52.
- Nimish, G., Chandan, M. C., & Bharath, H. A. (2018). UNDERSTANDING CURRENT AND FUTURE LANDUSE DYNAMICS WITH LAND SURFACE TEMPERATURE ALTERATIONS: A CASE STUDY OF CHANDIGARH. ISPRS Annals of Photogrammetry, Remote Sensing & Spatial Information Sciences, 4(5).
- Nimish, G., Chandan, M. C., & Bharath, H. A. (2018). UNDERSTANDING CURRENT AND FUTURE LANDUSE DYNAMICS WITH LAND SURFACE TEMPERATURE ALTERATIONS: A CASE STUDY OF CHANDIGARH. ISPRS Annals of Photogrammetry, Remote Sensing & Spatial Information Sciences, 4(5).
- Barsi, J. A., Schott, J. R., Hook, S. J., Raqueno, N. G., Markham, B. L., & Radocinski, R. G. (2014). Landsat-8 thermal infrared sensor (TIRS) vicarious radiometric calibration. Remote Sensing, 6(11), 11607-11626.

- Reddy, S. N., & Manikiam, B. (2017). Land surface temperature retrieval from LANDSAT data using emissivity estimation. International Journal of Applied Engineering Research, 12(20), 9679-9687.
- Sobrino, J. A., Jiménez-Muñoz, J. C., Sòria, G., Romaguera, M., Guanter, L., Moreno, J., ... & Martínez, P. (2008). Land surface emissivity retrieval from different VNIR and TIR sensors. IEEE Transactions on Geoscience and Remote Sensing, 46(2), 316-327.
- Jiménez-Muñoz, J. C., & Sobrino, J. A. (2008). Split-window coefficients for land surface temperature retrieval from low- resolution thermal infrared sensors. IEEE geoscience and remote sensing letters, 5(4), 806-809.
- Barsi, J. A., Schott, J. R., Hook, S. J., Raqueno, N. G., Markham, B. L., & Radocinski, R. G. (2014). Landsat-8 thermal infrared sensor (TIRS) vicarious radiometric calibration. Remote Sensing, 6(11), 11607-11626.
- Lu, D., & Weng, Q. (2006). Spectral mixture analysis of ASTER images for examining the relationship between urban thermal features and biophysical descriptors in Indianapolis, Indiana, USA. Remote Sensing of Environment, 104(2), 157- 167.
- Mallick, J., Singh, C. K., Shashtri, S., Rahman, A., & Mukherjee, S. (2012). Land surface emissivity retrieval based on moisture index from LANDSAT TM satellite data over heterogeneous surfaces of Delhi city. International Journal of Applied Earth Observation and Geoinformation, 19, 348-358.
- Mohan, M., Pathan, S. K., Narendrareddy, K., Kandya, A., & Pandey, S. (2011). Dynamics of urbanization and its impact on land-use/land-cover: a case study of megacity Delhi. Journal of Environmental Protection, 2(09), 1274.
- Salih, M. M., Jasim, O. Z., Hassoon, K. I., & Abdalkadhum, A. J. (2018). Land Surface Temperature Retrieval from LANDSAT-8 Thermal Infrared Sensor Data and Validation with Infrared Thermometer Camera. International Journal of Engineering & Technology, 7(4.20), 608-612.
- Orhan, O., & Yakar, M. (2016). Investigating land surface temperature changes using Landsat data in Konya, Turkey. International Archives of Photogrammetry, Remote Sensing and Spatial Information Sciences, 41, B8.
- Orhan, O., Ekercin, S., Dadaser-Celik, F., (2014) Use of Landsat Land Surface Temperature and Vegetation Indices for Monitoring Drought in the Salt Lake Basin Area, Turkey, The Scientific World Journal, vol. 2014, Article ID 142939, 11 pages.doi:10.1155/2014/142939
- Rajeshwari, A., & Mani, N. D. (2014). Estimation of land surface temperature of Dindigul district using Landsat 8 data. International Journal of Research in Engineering and Technology, 3(5), 122-126.
- Zhibin, R., Haifeng, Z., Xingyuan, H., Dan, Z., & Xingyang, Y. (2015). Estimation of the relationship between urban vegetation configuration and land surface temperature with remote sensing. Journal of the Indian Society of Remote Sensing, 43(1), 89-100.
- Sobrino, J. A., Jiménez-Muñoz, J. C., & Paolini, L. (2004). Land surface temperature retrieval from LANDSAT TM5. Remote Sensing of environment, 90(4), 434-440.
- Stathopoulou, M., & Cartalis, C. (2007). Daytime urban heat islands from Landsat ETM+ and Corine land cover data: An application to major cities in Greece. Solar Energy, 81(3), 358-368.
- Avdan, U., & Jovanovska, G. (2016). Algorithm for automated mapping of land surface temperature using LANDSAT 8 satellite data. Journal of Sensors, 2016.
- USGS,http://landsat.usgs.gov/Landsat8_ Using_Product.php, 2013.

- Wang, F., Qin, Z., Song, C., Tu, L., Karnieli, A., & Zhao, S. (2015). An improved mono-window algorithm for land surface temperature retrieval from Landsat 8 thermal infrared sensor data. Remote sensing, 7(4), 4268-4289.
- Weng, Q., & Lu, D. (2008). A sub-pixel analysis of urbanization effect on land surface temperature and its interplay with impervious surface and vegetation coverage in Indianapolis, United States. International journal of applied earth observation and geoinformation, 10(1), 68-83.
- Weng, Q., Lu, D., & Schubring, J. (2004). Estimation of land surface temperature–vegetation abundance relationship for urban heat island studies. Remote sensing of Environment, 89(4), 467-483.
- Yan, P., Shi, P., Gao, S., Chen, L., Zhang, X., & Bai, L. (2002). 137Cs dating of lacustrine sediments and human impacts on Dalian Lake, Qinghai Province, China. Catena, 47(2), 91-99.
- Yıldırım, Ü., Erdoğan, S., & Uysal, M. (2011). Changes in the coastline and water level of the Akşehir and Eber Lakes.